RESEARCH PAPER

Structural, Spectroscopic, and Quantum Computational Analysis of Methyl 1,3-Diphenyl-1H-Naphthol[2,1-b]Pyran -2-carbodithioates: DFT, ADME and Molecular Docking Studies.

Kshetrimayum Ameeta Devi[1], N. Shubhaschandra Singh[1]*

[1]*Department of Chemistry, Dhanamanjuri University Manipur-795001, India*
Corresponding author:
Email ID : shubhasnaorem@gmail.com or shubhashnaorem@dmu.ac.in (N. Shubhaschandra Singh), ORCID: 0000-0003-0479-9123

ABSTRACT
Medicinal and aromatic plants serve as valuable reservoirs of bioactive molecules and mineral compounds that are harnessed for therapeutic and agro-food applications. The study focuses on the structural and spectroscopic properties of a napthopyran derivative known as Methyl 1,3-diphenyl-1H-naphtho [2, 1-b] pyran-2-carbodithioate. This work presents the first quantum computational and systematic ADME/molecular docking analysis of methyl 1,3-diphenyl-1H-naphtho[2,1-b]pyran-2-carbodithioate, a compound not previously reported in this context. The study investigated electronic properties through several approaches, such as the frontier orbital (HOMO/LUMO), electronic properties, Electronic potential map, Fukui functions, Localized Orbital Locator (LOL), and electron density iso-surfaces. The compound exhibits substantial stability as shown by its large HOMO-LUMO gap and a favorable, moderate dipole moment. Docking and ADME analysis suggest potential as a lead for MMP-13 inhibition, with rational implications for drug design. The results indicate highly stable and unreactive, supported by the observed Electronic energy gap and a moderate dipole moment. Molecular docking analysis indicates a potential interaction with metalloproteinase (MMP)-13. Additionally, the naphthopyran derivative presents pharmacokinetic concerns.
Keywords: Molecular docking FT-IR, NMR, UV-Vis, DFT, MEP, B3LYP, LOL, Fukui Function, Molecular Docking etc
How to cite this article: Devi KA, Singh NS, Structural, Spectroscopic, and Quantum Computational Analysis of Methyl 1,3-Diphenyl-1H-Naphthol[2,1-b]Pyran -2-carbodithioates: DFT, ADME and Molecular Docking Studies...Int J Drug Deliv Technol. 2026; 16(8s): 339-356; DOI: 10.25258/ijddt.16.8s.46
Source of support: Nil.
Conflict of interest: None

INTRODUCTION

Naphthopyrans exhibit various biological activities, including anti-swelling, antimicrobial, cytostatic, analgesic, anticancer, cytotoxic effects1 etc. They belong to the category of photochromic compounds2,3. with applications spanning eyeglasses, electronic displays, optical switches, and temporary and permanent storage devices4. Consequently, synthesising the heterocyclic compound holds great significance5.

In recent years, chemists have increasingly turn to computational and theoretical methods. Density Functional Theory (DFT) stands out for its precision in analysing molecular vibrations, thermodynamic properties, and electronic characteristics of organic compounds. Surprisingly, there have been no prior quantum computational studies of methyl 1,3-diphenyl-1H-naphtho [2, 1-b] pyran-2-carbodithioates1, making it a fascinating topic for quantum computational analysis. In order to incorporate such analysis, this study used B3LYP/6-311++G(d,p) method6. The comprehensive examination of quantum computational analysis in this study comprises energy levels, molecular structures, charge distributions, vibrational modes, electronic spectra and magnetic resonance parameters7. To the best of our knowledge, no DFT or quantum computational studies on this specific carbodithioate system have been previously reported.

METHODOLOGY

Computational Method

DFT calculations were performed using the B3LYP/6-311++G (d,p) level. All structures were optimized and vibrational frequencies, molecular orbitals, and reactivity indices were calculated with strict convergence criteria. In this Quantum computational study, the ORCA 6.1 package was utilised (supported by Avogadro) 8. The level of study of B3LYP/6-311++G (d,p) level 6 was used to establish the most stable geometry for the synthesised derivative (4). The optimised one that is the most stable was used to analyse vibrational peaks and chemical shifts 9,10 of NMR peaks in the in silico study.

We also performed calculations for FMO, MEP, atomic charge density (ACD), Fukui functions, LOL, and constant height scanning tunnelling microscopy (STM) images 11. The potential electronic distribution (PED) for each vibrational mode was determined using the VEDA program 12,13. Furthermore, in silico calculations of LOL, STM, and density of iso-surfaces were performed using Multiwfn 3.8 14 at the same level of theory.

**Author for Correspondence: Kshetrimayum Ameeta Devi*

In silico ADME and Target Prediction

In silico screening of the synthesised Methyl 1,3-diphenyl-1H-naphtho [2, 1-b] pyran-2-carbodithioate) for Absorption, Distribution, Metabolism, and Excretion (ADME) properties, evaluation of drug-likeness for biological targets prediction was conducted using the open-source tools SwissADME and SwissTargetPrediction15,16. Fundamental physicochemical parameters such as molecular weight (MW), molecular refractivity (MR), topological polar surface area (TPSA), and atom counts, were accurately computed during the analysis. The properties of drug-likeness of the synthesised derivative (4) were assessed based on Lipinski17, Ghose18, Veber19, Egan20 and Muegge21 rules. Abbot's bioavailability score was used to estimate of achieving at least 10% oral bioavailability by considering the total charge. Lipophilicity was determined using multiple prediction models such as iLOGP, SILICOS-IT, MLOGP, and XLOGP3, leading to a consensus Log $P_o/_x$ value15,16. Three other models were also used to predict the chosen ligands' aqueous solubility (log S): ESOL22, Ali23 and SILICOS-IT16.

In silico Molecular Docking

SwissADME16 was utilized to select and evaluate the target protein. The protein was prepared and minimized using Discovery Studio following standard protocols. The prepared receptors were then subjected to docking with the ligand, targeting on their active sites. This ligand-receptor interaction was carried out using the Click-1 interface available on Mcule. Methyl 1,3-diphenyl-1H-naphtho [2, 1-b] pyran-2-carbodithioate was synthesised based on the established procedure1 as illustrated in Scheme 1.

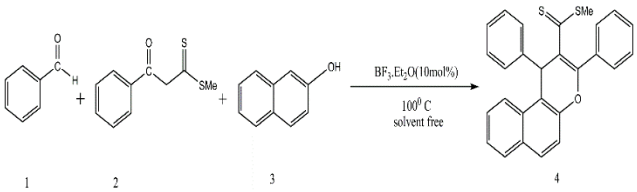

Scheme 1. Synthesis of Methyl 1,3-diphenyl-1H-naphtho[2,1-b]pyran-2-carbodithioate

Shidmazu FTIR-8400S spectrophotometer and FT-NMR-DRX 400 (Bruker Advance spectrometer) were used to report the spectral data of the synthesised compound. IR spectrum of the compound showed characteristic peaks at 428, 501, 629, 1005, 1045, 1192, 1323, 1400, 1492, 1595, 1639 cm-1. The ^{1}H NMR spectrum reported peaks at 8.35 ppm (doublet, J = 8.0 Hz, 2H), 7.88–7.86 ppm (multiplet, 4H), 7.77–7.64 ppm (multiplet, 5H), 7.56–7.05 ppm (multiplet, 5H), 5.94 ppm (singlet, 1H), and 2.31 ppm (singlet, 3H). The 13C NMR spectrum included peaks at 232.68 (C=S), 153.28, 148.41, 146.20, 143.96, 138.87, 136.89, 135.27, 134.51, 133.02, 132.32, 131.07, 129.99, 129.29, 129.00, 128.40, 128.15, 126.92, 125.32, 123.74, 123.13, 121.14, 120.53, 116.13, 112.93, 38.09, 20.85.

Results and Discussion

Electron Characterization

The optimized geometry of the Methyl 1,3-diphenyl-1H-naphtho[2,1-b]pyran-2-carbodithioate is shown in Figure 1, and the computed global parameters24 are reported in Table 1. The energy of LUMO (ELUMO) and HOMO (EHOMO) and E_g (difference of ELUMO and EHOMO) are estimated as -0.08443, -0.21857, and 0.13414 a.u respectively (Figure 2). Since the E_g value exceeds 0.1au, the derivative exhibits a high HOMO-LUMO gap, indicating stability and low reactivity25,26. The dipole moment for the compound is 1.957767 D, suggesting moderate polarity due to uneven electron distribution among its atoms27.

Analyzing the HOMO and LUMO patterns (Figure 2), the HOMO is found distributed throughout the molecule except for the phenyl groups attached to C13 and C11. This region is reactive toward electrophiles. Conversely, the LUMO is primarily localised on sulphur atoms and adjacent atoms, extending to other positions excluding the phenyl ring connected to C13. The LUMO region is reactive towards nucleophiles. The MEP map of the synthesised compound is shown in Figure 3. The potential distribution is depicted using a colour gradient28,29. In this scheme, red highlights areas with high nucleophilic reactivity, while blue signifies regions with strong electrophilic character. The intermediate hues—light blue, green, and yellow—stand for slightly electron-deficient, neutral, and electron-rich regions, respectively. Notably, red colour appears on S33 atoms and near O20. It also occurs between the naphthalene plane and the phenyl ring attached to C-13. Blue colour is associated with the H36 atoms of the methyl group connected to S49 naphthalene ring plane.

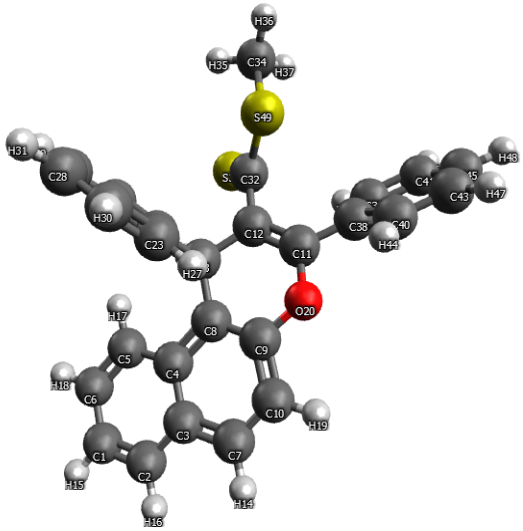

Figure 1. The optimised geometry of Methyl 1,3-diphenyl-1H-naphtho[2,1-b]pyran-2-carbodithioate

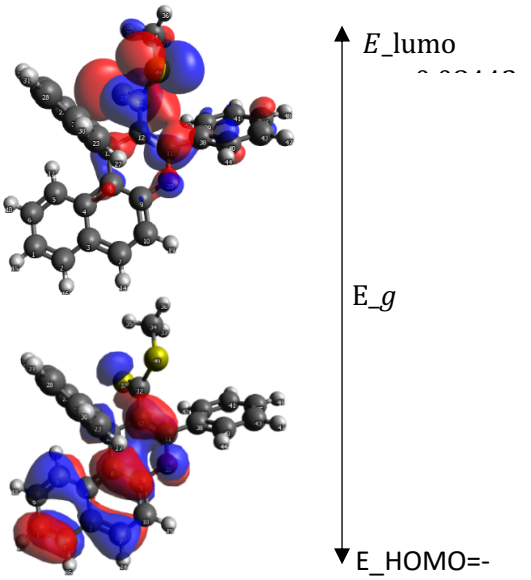

Figure 2. Calculated EHOMO, ELUMO of Methyl 1,3-diphenyl-1H-naphtho[2,1-b]pyran-2-carbodithioate using B3LYP/3-611G++(d,p)

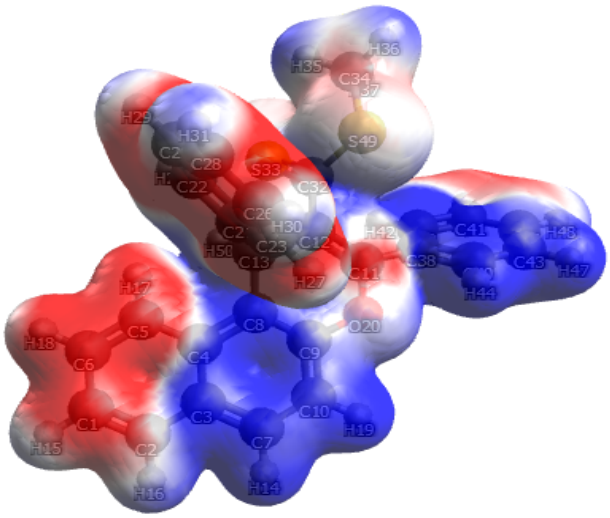

Figure 3. MEP of Methyl 1,3-diphenyl-1H-naphtho[2,1-b]pyran-2-carbodithioate using B3LYP/3-611G++(d,p)

Table 1. Calculated Global Parameters of Methyl 1,3-diphenyl-1H-naphtho[2,1-b]pyran-2-carbodithioate

Parameter	compound in Gaseous state	
	Basis set	
	6-311G++(d,p)	6-31G++(d,p)
EHOMO	-0.2186	-0.21661
ELUMO	-0.0844	-0.08382
ELUMO - EHOMO	0.1341	0.13279
Ionization potential (a.u)	0.2186	0.21661
Electron affinity (A a.u)	0.0844	0.08382
Electronegativity (□□ a.u)	0.1515	0.15022
Chemical hardness □□, a.u)	0.0671	0.06640
Chemical softness (□, a.u)	7.4549	7.53069
Electrophilicity index (□, a.u)	0.1711	0.16993

FTIR analysis

The theoretical vibrational frequencies and associated infrared intensities of the optimised structure of the Methyl 1,3-diphenyl-1H-naphtho[2,1-b]pyran-2-carbodithioate are shown in Figure 4. These results, together with the energy topology called PED analysis30, are presented in Table 2.

The PED analysis quantifies the contribution of specific atomic movements in normal mode12,13.

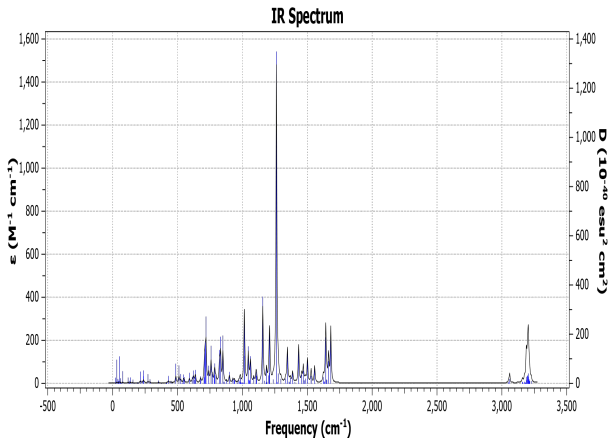

Figure 4. Calculated IR spectra for Methyl 1,3-diphenyl-1H-naphtho[2,1-b]pyran-2-carbodithioate using B3LYP/3-611G++(d,p) method

The optimised structure of the Methyl 1,3-diphenyl-1H-naphtho[2,1-b]pyran-2-carbodithioate exhibits a total of 144 vibrational normal modes. These include 49 stretching (ν), 48 bending (β), and 47 torsional modes (τ)29. Vibrational mode assignment uses the same level of theory as that of optimisation of the derivative. Every one of the 144 basic vibrational modes is active in the infrared spectrum. Notably, the experimentally observed frequencies at 728, 1323, and 1639 cm^{-1} were assigned to stretching modes by using the PED analysis (Table 2). The remaining experimentally observed frequencies at 501, 629, 1005, 1045, 1192, 1400, 1492 and 1595 cm^{-1} were assigned to distinct modes, showing differences within ±3 cm^{-1} in the Table 2 following PED analysis without empirical scaling factors to account for anharmonic effects.

Table 2. Calculated frequencies, intensities and PED analysis of Methyl 1,3-diphenyl-1H-naphtho[2,1-b]pyran-2-carbodithioate using B3LYP/3-611G++(d,p) level

Frequencies (cm-1)	Intensity	PED Contribution (%)
3208.25	5.39	92 ν(C5H17)
3197.52	5.94	90 ν (C10H19)
3195.54	6.09	91 ν(C39H42)
3192.3	10.52	81 ν_{as} (C39H42) + 15 ν_{as}(C41H46)
3188.77	17.54	77 ν (C26H30)
3186.46	28.36	12 ν (C1H15) + 78 ν (C1H15)
3183.87	21.82	91 ν_{as} (C39H42)
3179.31	20.43	12 ν_{as} (C26H30) + 76 ν_{as} (C22H25)
3172.72	8.16	17 ν (C39H42) + 82 ν_{as}(C41H46)
3172.21	10.36	91 ν(C22H2)
3171.31	18.36	90 ν(C1H15)
3169.24	0.83	90 ν(C6H18)
3163.48	0.75	73 ν(C22H25)
3163.44	0.22	88 ν_{as}(C22H25)
3159.24	2.15	84 ν_{as}(C1H15) + 14 ν(C1H15)
3157.71	3.01	87 ν(C22H25)

3142.97	2.05	96 ν_{as} (C34H35)
3140.18	3.45	96 ν (C34H36)
3048.04	11.44	98 ν(C34H35)
3042.44	3.08	100 ν(C13H50)
1675.8	77.77	61 ν(C11C12)
1656.33	33.53	25 ν_{as}(C1C2) + 14 ν_{as} (C7C10) + 12 ν (C5C4)
1642.72	5.74	48 ν_{as}(C40C43)+18 β_{as} (H42C39C 41)
1639.8	5.58	43 ν (C23C26)+ 17 β(H30C26C28)
1635.06	67.65	41 ν (C7C10)
1624.28	1.82	32 ν_{as} (C26C28)
1621.23	1.57	14 ν_{as} (C8C9) + 19 ν_{as} (C26C28)
1615.51	7.74	57 ν_{as}(C41C45)
1549.67	22.74	26 ν(C1C6) + 12 β_{as} (H14C7C10) + 18 β(H16C2C1)
1524.55	7.53	11 ν(C39C41) +56 β(H46C41C45)+ 15 β (C40C43C45)
1523.51	11.82	60 β(H25C22C24)
1495.81	28.05	11 ν_{as}(C1C6,C1C2) + 11 ν (C5C4)+ 10 β(H14C7C10) + 21 β(H14C7C10)
1483.08	7.1	18 ν(C22C24) + 54 β_{as} (H31C28C26)
1474.6	4.08	23 ν_{as}(C39C41) + 11 β_{as} (H42C39C41) +46 β_{as} (H48C45C43)
1463.97	19.24	11β(H14C7C10) + 31 β(H16C2C1) + -13 β(H35C34H37)
1463.36	4.8	45 β (H35C34H37) +-18 τ (H42C39C41C45, H44C40C43C45, H46C41C45C43, H47C43C45C41),
1451.07	12.81	36 β_{as}(H36C34H35) + 37 β(H37C34H36), 10 τ (H37C34S49C32, H35C34S49C32) + -17 τ (H36C34S49C32)
1424.28	48.21	24 ν (C8C9) + 13 β(C3C2C1)
1396.88	3.82	15 ν (C4C8) +12β_{as}(H14C7C10, H19C10C7)
1378.78	9.6	20 ν(C1C2) +10 β_{as}(C3C2C1) + 16 β_{as}(H50C13C21, H27C23C26, H25C22C24, H30C26C28, H29C24C28, H31C28C26)
1367.65	8.96	69 β (H50C13C21, H27C23C26, H25C22C24, H30C26C28, H29C24C28)

1356.03	1.18	12 ν(C38C39) 78 + β(H42C39C41, H44C40C43, H46C41C45, H47C43C45)
1353.09	0.43	-24 β_{as}(H35C34H37) +35β_{as}(H36C34H35) + 34 β_{as}(H37C34H36)
1345.99	4.18	44 ν_{as}(C26C28) + 25 β_{as}(H50C13C21, H27C23C26, H25C22C24)
1341.13	34.63	13 ν_{as} (C38C11)+ -11 s75 (bend C12C11O20), -23 s106 (tors H42C39C41C45, H44C40C43C45, H46C41C45C43)
1322.61	1.14	57 ν(C38C39)
1294.23	4.85	11 ν (C5C4) + 40 β_{as} (H17C5C6)
1271.25	8.03	14 ν_{as}(C26C28) + 41 β(H50C13C21)
1264.98	5.57	-22 τ (H50C13C21C22)
1249.47	418.95	44 ν(O20C9)
1232.59	3.69	10 ν_{as}(C1C6) + 17 β_{as}(H14C7C10)
1206.3	54.16	16 ν(C32C12)+ 26 β(H42C39C41)
1205.57	0.18	15 ν_{as}(C23C26) + 68β(H30C26C28)
1204.04	22.04	42 β (H42C39C41, H44C40C43, H46C41C45, H47C43C45)
1199.24	11.76	14 ν(C32C12) + 18 ν(C13C21)
1186.33	0.9	13 ν_{as}(C13C21)
1183.35	16.99	58 β (H18C6C1, H15C1C2, H17C5C6, H19C10C7, H47C43C45, H46C41C45)
1183.03	3.16	75 β(H48C45C43, H47C43C45, H46C41C45)
1181.18	0.16	13 ν_{as}(C26C28) + 73 β (H31C28C26, H29C24C28, H30C26C28)
1166.45	2.87	62 β(H19C10C7, H15C1C2, H16C2C1, H14C7C10)
1151.09	120.59	19 ν(C9C10) + 12 β(C12C11O20)
1106.79	9.17	18 ν_{as}(C22C24) + 14 ν_{as}(C39C41) + 19 β_{as}(H31C28C26, H27C23C26, H29C24C28, H30C26C28, H25C22C24) + 12 β (H48C45C43, H47C43C45, H42C39C41)
1102.99	13.46	15 ν_{as}(C22C24) + 26 ν(C39C41) +13 β_{as} (H31C28C26, H27C23C26, H29C24C28, H30C26C28, H25C22C24) + 21 β_{as}(H48C45C43, H47C43C45, H42C39C41)
1085.09	7.49	12 ν(C8C13) + 10 β(C3C2C1) + 11 β_{as} (H14C7C10, H16C2C1, H18C6C1)

1059.76	25.11	12 β(H46C41C45,H44C40C43,) + 13 β_{as} (C40C43C45, C41C45C43,)
1052.76	1.63	42 ν(C1C6)
1049.42	3.95	40 ν(C26C28) + 17 β(H25C22C24, H27C23C26) + 15 β_{as} (C23C26C28, C22C24C28)
1042.65	42.75	18 ν(C43C45) +13 ν (C9C10) +14 ν(S33C32) +10 β_{as}(C40C43C45, C41C45C43)
1017.14	1.15	13 ν(C23C26) + 22 ν(C24C28) + 19 β_{as} (C24C28C26) + 37β(C23C26C28)
1016.07	6.87	42 ν(C43C45) + 43 β (C40C43C45, C41C45C43, C39C41C45)
1013.97	99.22	14 ν(S33C32) + 13β(C9C8C13) + 10 β(C11O20C9)
1009.14	0.36	61 τ(H48C45C43C40, H46C41C45C43, H47C43C45C41) + -29 τ (C39C41C45C43)
1003.11	0.74	-69 τ (H31C28C26C23, H30C26C28C24) +-24 τ (C22C24C28C26)
996.71	0.08	72 τ (H15C1C2C3, H18C6C1C2) + 15 τ (C2C1C6C5, C6C5C4C8)
991.89	0.81	81 τ(H42C39C41C45, H44C40C43C45) +-15 τ(C40C43C45C41, C39C41C45C43)
985.98	0.21	-83 τ (H25C22C24C28, H27C23C26C28,)+15 τ (C22C24C28C26, C23C26C28C24)
979.56	8.54	16 β(H35C34H37) +-66 τ(H37C34S49C32)
977.08	0.89	82 τ(H14C7C10C9)
967.45	2.67	12 β (H36C34H35) +12 β_{as}(H37C34H36) + -33 τ(H37C34S49C32, H35C34S49C32) + 43 τ (H36C34S49C32)
963.28	0.45	83 τ (H14C7C10C9, H15C1C2C3, H16C2C1C6, H17C5C6C1, H18C6C1C2)
942.21	3.53	81 τ (H42C39C41C45, H44C40C43C45, H48C45C43C40)
936.87	2.79	52 τ (H31C28C26C23, H25C22C24C28, H27C23C26C28)
925.6	5.24	-19 τ(H31C28C26C23, H25C22C24C28, H27C23C26C28)
899.71	10.13	11 ν_{as}(C8C13) + 26 β(C7C10C9)
875.83	1.87	62 τ (H17C5C6C1, H16C2C1C6) +-14 τ (C2C1C6C5, C3C2C1C6, C1C6C5C4)

858.95	0.87	97 τ (H42C39C41C45, H44C40C43C45, H46C41C45C43, H47C43C45C41)
856.07	1.43	95 τ (H25C27C24C28, H27C23C26C28, H29C24C28C26, H30C26C28C24)
849.7	38.94	12 β_{as}(C24C28C26)
830.73	41.02	19 τ(H14C7C10C9, H19C10C9C8)
822.67	30.86	33 τ (H14C7C10C9, H19C10C9C8)
797.77	8.33	11 τ (C2C1C6C5, C3C2C1C6, C1C6C5C4)
788.75	12.86	-15 τ (H48C45C43C40, H44C40C43C45)+-11 τ(C2C1C6C5, C3C2C1C6, C1C6C5C4) + 24 τ (C45C41C39C38)
784.15	5.11	13 τ (H31C28C26C23, H27C23C26C28, H30C26C28C24, H29C24C28C26)
768.47	6.06	14 τ (C2C1C6C5, C3C2C1C6, C1C6C5C4)
757.64	32.51	73 τ (H15C1C2C3)
741.29	11.89	
718.58	62.63	-40 τ (H31C28C26C23)
711.29	17.83	24 ν(S49C34) + -11 τ (H31C28C26C23) +13 τ(H31C28C26C23) + -30 τ (C21C22C24C28)
709.43	29.42	50 τ (H48C45C43C40)+21τ (C45C41C39C38)
704.82	1.49	45 ν(S49C34)
681.23	1.34	18 β(C41C46C43)
679.43	4.65	-10 τ (H14C7C10C9, H19C10C9C8)
639.63	8.52	14 β(C23C26C28, C22C24C28)
636.73	3.26	51 β(C40C43C45, C39C41C45)
631.75	2.47	53 β(C23C26C28, C22C24C28)
623.55	8.63	24 β_{as}(C40C43C45, C39C41C45)
591.48	6.26	15 ν_{as}(S49C32) +18 β(C11O20C9)
551.08	3.52	26 (out S33C12S49C32)
535.81	0.19	10 τ_{as}(C1C6C5C4) + 36 τ(C2C1C6C5) + 13 (out C10C8O20C9)
523.62	4.6	-10 (out C4C9C13C8)
511.36	10.05	10 τ (C39C41C45C43)
464.39	0.11	11β_{as} (C6C5C4) + 13 β(C5C4C8)

428.41	3.2	11β_{as}(S33C32S49) + 27 τ_{as}(C1C6C5C4)

Fukui Function

In the DFT method, molecular reactivity is assessed through the Fukui function. It assists in determining which parts of a molecule are most vulnerable to electrophilic and nucleophilic assaults and is represented by the symbol f(r)11,31. Mulliken population study is applied to calculate$f^+(r)$, $f^-(r)$ and $f^0(r)$ of the Methyl 1,3-diphenyl-1H-naphtho[2,1-b]pyran-2-carbodithioate and are presented in Table 3.

The $f^+(r)$, $f^-(r)$ and $f^0(r)$ are defined as follow:

$$f^+(r) = q_j(N+1) - q_j(N)$$

$$f^-(r) = q_j(N) - q_j(N-1)$$

$$f^0(r) = \frac{1}{2}\left[q_j(N+1) - q_j(N-1)\right]$$

According to the data, the C13 atom shows a higher susceptibility to cationic and neutral attacks, whereas C21 is more reactive under anionic conditions. These atoms are particularly susceptible to nucleophilic attacks32. The nucleophilic attack order for cationic, anionic and neutral is as follows: C12>C39>C13>C21>C5>C39>C1>C10. Atoms with Fukui index values close to zero are likely sites for radical attacks. In contrast, atoms carrying a negative charge tend to be more reactive toward electrophilic attack. Notably, nucleophilic attacks generally show higher reactivity than both electrophilic and radical interactions.

Table 3. Calculated $\boldsymbol{f^+(r)}$, $\boldsymbol{f^-(r)}$ and $\boldsymbol{f^0(r)}$ of Methyl 1,3-diphenyl-1H-naphtho[2,1-b]pyran-2-carbodithioate using B3LYP/3-611G++(d,p) method

Atom	$\boldsymbol{f^+(r)}$	$\boldsymbol{f^-(r)}$	$\boldsymbol{f^0(r)}$
C1	-0.111	0.23	0.0595
C2	0.168	-0.118	0.025
C3	-0.19	0.049	-0.0705
C4	-0.029	0.176	0.0735
C5	0.305	-0.09	0.1075
C6	-0.112	-0.139	-0.1255
C7	0.04	0.01	0.025
C8	-0.109	0.167	0.029
C9	-0.112	-0.275	-0.1935
C10	0.222	-0.157	0.0325
C11	-0.192	-0.001	-0.0965
C12	-0.221	0.165	-0.028
C13	0.828	-0.004	0.412
H14	-0.025	-0.057	-0.041
H15	-0.029	-0.055	-0.042
H16	-0.025	-0.056	-0.0405
H17	0.011	-0.246	-0.1175
H18	-0.02	-0.054	-0.037
H19	-0.022	-0.062	-0.042
O20	-0.044	0.033	-0.0055
C21	-0.213	0.32	0.0535
C22	0.177	0.014	0.0955
C23	-0.143	-0.001	-0.072
C24	-0.077	0.068	-0.0045
H25	-0.03	-0.023	-0.0265
C26	0.203	-0.019	0.092
H27	-0.005	-0.041	-0.023
C28	-0.032	0.175	0.0715
H29	-0.025	-0.059	-0.042
H30	-0.027	-0.064	-0.0455
H31	-0.035	-0.059	-0.047
C32	-0.137	-0.217	-0.177
S33	-0.384	-0.401	-0.3925

C34	-0.079	0.124	0.0225
H35	-0.055	-0.023	-0.039
H36	-0.042	-0.058	-0.05
H37	-0.034	-0.039	-0.0365
C38	-0.408	0.073	-0.1675
C39	0.443	0.057	0.25
C40	-0.187	-0.02	-0.1035
C41	-0.124	-0.028	-0.076
H42	0.047	-0.031	0.008
C43	0.039	0.011	0.025
H44	-0.024	-0.062	-0.043
C45	-0.16	0.13	-0.015
H46	-0.038	-0.062	-0.05
H47	-0.042	-0.069	-0.0555
H48	-0.048	-0.064	-0.056
S49	0.134	0.03	0.082
H50	-0.037	-0.08	-0.0585

Surface Map with Projected Localised Orbital Locator (LOL) Analysis

Multiwfn 3.814 is a robust tool in quantum chemistry for analysing electronic wave functions. It employs the Localised Orbital Locator (LOL) to generate shaded surface maps, which help visualize regions of rich electron density and electron deficiency. Localised Orbital Locator (LOL) defined by Eqn. 1, identifies localised high regions, where electron motion is likely restricted11. For the Methyl 1,3-diphenyl-1H-naphtho[2,1-b]pyran-2-carbodithioate, the LOL–projected shaded surface map (Figure 5) provides key insights: Blue circular zones surrounding the nuclei signify areas with significant electron depletion, typically found between the valence and inner electron shells, and are especially noticeable within the naphthalene rings.

$$LOL(r) = \frac{\tau(r)}{1+\tau(r)} \qquad \text{Eqn. 1}$$

Where $\tau(r)$(dimensonless variable) is $g_0(r)/g(r)$ and $g(r) =$ is density of kinetic energy.

In contrast, red-colored regions highlight zones of strong electron localisation. Electrons are primarily localised on the molecule's outer regions, contributing to its structural stability.

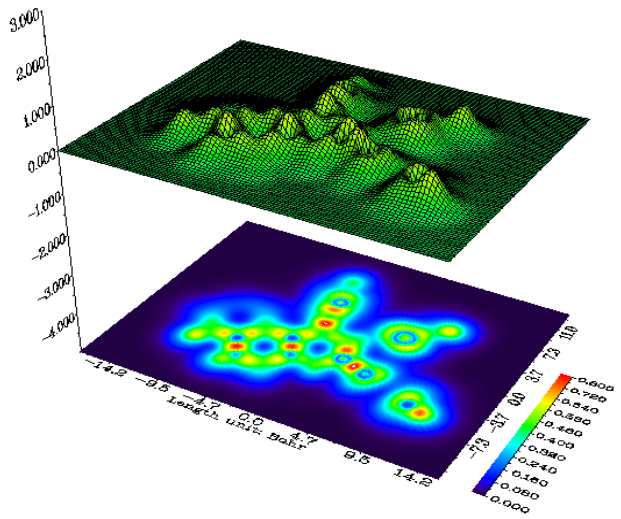

Figure 5. LOL-projected shaded surface map of Methyl 1,3-diphenyl-1H naphthol[2,1-b]pyran-2-carbodithioate

Density of Iso-Surface Electrons

The molecular density of iso-surface electrons of the Methyl 1,3-diphenyl-1H naphthol[2,1-b]pyran-2-carbodithioate was analysed using Multiwfn 3.8 software. Table 4 presents the maximum and minimum energy values identified during the analysis. The atom with the highest energy is S49 (maxima), recorded at 2567.019 kcal/mol, while the lowest is S33 (minima), with an energy of 2409.618 kcal/mol. Figure 6 presents a visual representation of this analysis.

Table 4. Maxima and minima iso-surface value of Methyl 1,3-diphenyl-1H-naphtho[2,1-b]pyran-2-carbodithioate

Maxima Iso-Surface		Minima Iso-Surface	
Specific Atom	Energy (kcal/mol)	Specific Atom	Energy (kcal/mol)
S49	2567.019	S33	2409.618
S33	2516.693	O20	712.063
O20	1054.925		

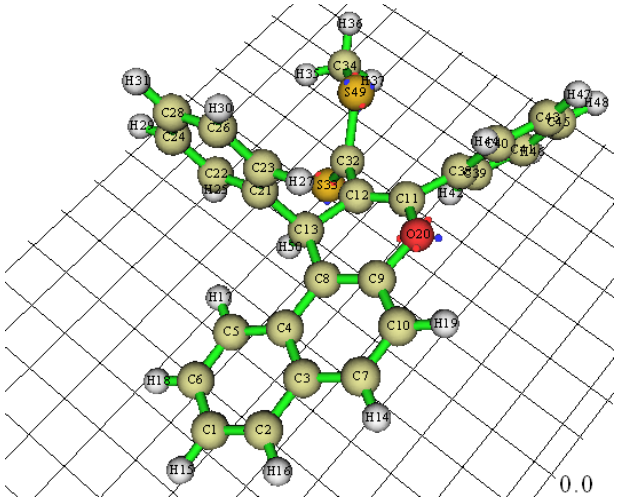

Figure 6. Maxima and minima iso-surface value of Methyl 1,3-diphenyl-1H-naphtho[2,1-b]pyran-2-carbodithioate

Constant Height STM Image Simulation

The simulated Scanning Tunnelling Microscope (STM) image was generated using Multiwfn 3.8 and is presented in Figure 7. The computed maximum LDOS is 0.000214 a.u. The brighter white regions represent areas of higher LDOS, which correspond to stronger tunnelling currents (I). According to the Tersoff-Hamann model33, the tunnelling current varies with LDOS. It is observed that the tunnelling current appears to be most significant around the benzene ring, particularly at the C21 and H50 atomic sites.

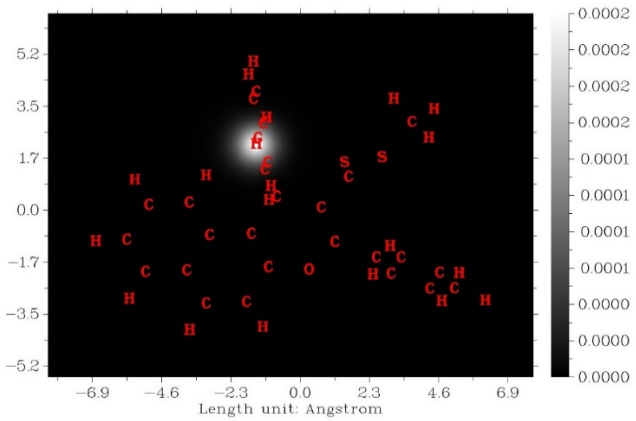

Figure 7. Scanning Tunneling Microscope (STM) image of Methyl 1,3-diphenyl-1H-naphtho[2,1-b]pyran-2-carbodithioate

Nuclear Magnetic Resonance (NMR) Analysis

Gauge-Including Atomic Orbital (GIAO) methodology is widely used for calculating chemical shifts34,35 in NMR spectra. The solvent effects are considered essential, as they impact molecular geometries and shielding constants. Density functional theory (DFT) is employed for precise and efficient NMR chemical shift calculations, and the NMR spectra with chemical shifts are shown in Figure 8 & 9. The analysis involves a 3×3 matrix derived from the chemical shift tensor34, which captures the anisotropy between the induced magnetic field (Bind) and the externally applied field (B0). Table 5 presents the computed and observed chemical shift values for both 1HNMR and 13CNMR data of the Methyl 1,3-diphenyl-1H-naphtho[2,1-b]pyran-2-carbodithioate in DMSO solution using TMS as referencing standard. Table 6 also lists the specific chemical shift assignments for both 1H and 13C nuclei in in the compound dissolved in DMSO. The 13C NMR data indicate that carbon C32 has the highest chemical shifts i.e., deshielding (around □□256 ppm) (Figure 9). This de-shielding effect may result from reduced electron density around C32 due to factors like electronegative groups (S33), methoxy sulphur (S49), sp2 hybridization, magnetic anisotropy, or steric effects. Similarly, for 1HNMR, H14 shows the highest deshielding (chemical shift of 8.36 ppm) and is located in the naphthalene ring bonded to C7 (Figure 8) thus highlighting the sensitivity of NMR shifts to aromatic ring current and electronic environment. Overall, the close correspondence between computational and experimental results demonstrates that DFT-GIAO methods, especially when solvent effects are considered, deliver consistent and reliable NMR predictions for structurally complex naphthopyran derivatives i.e., Methyl 1,3-diphenyl-1H naphthol[2,1-b]pyran-2-carbodithioate.

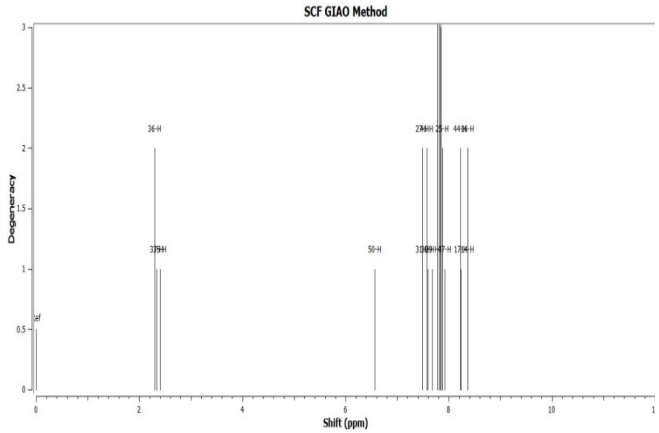

Figure 8. Calculated 1H NMR of the Methyl 1,3-diphenyl-1H-naphtho[2,1-b]pyran-2-carbodithioate

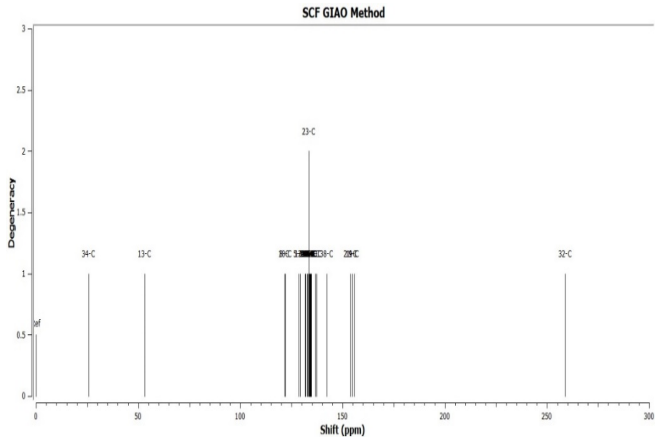

Figure 9. Calculated 1C NMR of the Methyl 1,3-diphenyl-1H-naphtho[2,1-b]pyran-2-carbodithioate

Table 5. Chemical shift of the Methyl 1,3-diphenyl-1H-naphtho[2,1-b]pyran-2-carbodithioate in DMSO solution, δ (ppm)

Shift values (□□□ppm)			
*Theor. (13H NMR)	*Expt. (13H NMR)	*Theor. (13C NMR)	*Expt (13C NMR)
8.36 (2H)	8.35 (2H)	259	232.68 (C=S),
		155.57	153.28
8.23 (2H)	7.88-7.86 (m, 4H)	154.68	148.41
		153.77	146.20
7.84(7H)		142.16	143.96
7.67(1H)	7.77-7.64 (m, 5H)	137.33	138.87
7.58(2H)	7.56-7.05 (m, 5H)	136.46	136.89
7.48(2H)		134.58	135.27
6.56 (1H)	5.94 (s, 1H)	134.45	134.51
2.39(1H)		134.34	133.02
2.31(2H)	2.31(s, 3H)	134.03	132.32
		133.94	131.07
		133.71	129.99
		133.45	129.29
		132.92	129.00
		132.82	128.40
		131.81	128.15
		131.67	126.92
		129.171	125.32
		128.44	123.74
			123.13
		121.79	121.14
		121.55	120.53
			116.13
			112.93
		53.09	38.09
		25.71	20.85
*Theor. = Theoretical; *Expt.= Experimental			

Table 6. Chemical shifts assignment of the Methyl 1,3-diphenyl-1H-naphtho[2,1-b]pyran-2-carbodithioate in DMSO solution, δ (ppm)

Atom position.	Shift value (□□ ppm)	Atom Position	Shift value (□□□ppm)
H14	8.36	C1	129.171
H15	7.84	C2	133.94
H16	8.36	C3	137.33
H17	8.23	C4	136.46
H18	7.84	C5	128.44
H19	7.84	C6	131.81
H25	7.84	C7	134.58
H27	7.48	C8	121.55
H29	7.67	C9	155.57
H30	7.58	C10	121.79
H31	7.48	C11	154.68
H35	2.39	C12	133.45
H36	2.31	C13	53.09
H37	2.31	C21	153.77
H42	7.84	C22	134.34
H44	8.23	C23	133.45
H46	7.58	C24	132.82
H47	7.84	C26	134.45
H48	7.84	C28	131.67
H50	6.56	C32	259
		C34	25.71
		C38	142.16
		C39	133.09
		C40	133.71
		C41	132.92
		C43	134.03
		C45	134.13

Calculated Atomic Charges

Population analysis divides the molecular wave-function into atom contributions to evaluate atomic charges. These charges are often computed as Mulliken charges and are illustrated in Figure 10. To improve the reliability of these charges for the basis set, Löwdin35 suggested orthogonalizing the atomic orbital basis functions before performing the analysis. For the compound Methyl 1,3-diphenyl-1H naphthol[2,1-b]pyran-2-carbodithioate, the total charges were calculated to be zero (0). Specifically, the most positively charged atom is C38, which is attached to benzene ring 1, while the most negatively charged atom is C39, also attached to the same benzene ring 1.

Pharmacokinetic Study

Assessment of the ADME characteristics of the Methyl 1,3-diphenyl-1H-naphtho[2,1-b]pyran-2-carbodithioate was carried out using the SwissADME16. The bioavailability radar indicated a drug-like physicochemical environment for oral activity; however, the compound's properties fell outside this zone it may not be orally active (Figure 11). Here, LIPO, POLAR, INSOLU, INSATU and FLEX are read as lipophilicity, polarity, insolubility, insaturation and flexibility. Key physicochemical properties include high lipophilicity (above 5), near insolubility in water, and a bioavailability score of 0.55 presented in Table 7 (within Lipinski17 and Veber19 filters. While the compound can be synthesised its limited gastrointestinal absorption and lack of blood-brain barrier permeability may hinder its progression in drug development. Additionally, it acts as a substrate for permeability glycoprotein (P-gp), potentially leading to efflux from the gastrointestinal tract or brain. Only the CYP2CP isoform interacts with the compound, implying involvement in biotransformation.

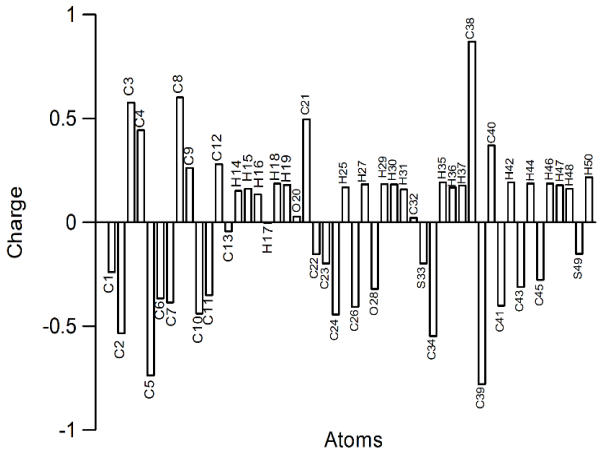

Figure 10. Atomic charge distribution of the Methyl 1,3-diphenyl-1H-naphtho[2,1-b]pyran-2-carbodithioate

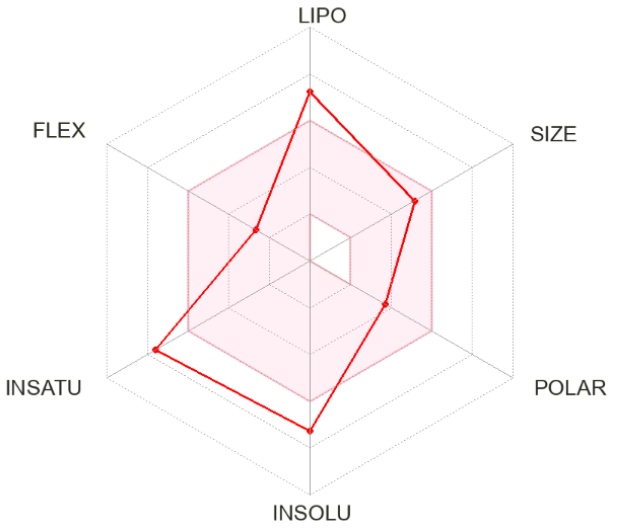

Figure 11. Bioavailability radar for Methyl 1,3-diphenyl-1H-naphtho[2,1-b]pyran-2-carbodithioate

Table 7. Basic physico-chemical properties and computed descriptor of Methyl 1,3-diphenyl-1H-naphtho[2,1-b]pyran-2-carbodithioate

Descriptor	Predicted value
Molecular weight	428.59 g/mol
No. of H-bond Acceptor	1
No. of H-bond Acceptor	0
Log Po/w (concensus)	6.29
Log S	-8.3933
TPSA	66.62Å2
Rule of five score	0.55

Molecular Docking

The molecular docking technique plays a critical role in drug development and computational chemistry5. In this study, the target receptor was selected using the SwissTargetPrediction platform, as visualized in the target pie chart (Figure 12) and the ranked list of predicted targets presented in Table 8. SwissTargetPrediction estimates the most likely protein targets for small molecules16, operating on the principle that structurally similar bioactive compounds often interact with similar biological targets. As such, the tool identifies potential targets by comparing the query molecule to known ligands with high structural similarity. The output includes a list of predicted protein targets along with their common names and direct links to external databases like GeneCards, UniProt, and ChEMBL. These targets are prioritized based on their similarity scores relative to the input compound.

Molecular docking estimates the most favourable alignment of a molecule relative to another when they form a stable complex, such as a protein–ligand36,37. Docking

simulations provide critical insights into ligand–receptor interactions, revealing details such as binding affinity and the types of intermolecular forces involving hydrogen linkages, London dispersion forces, and water-repelling effects37. Researchers analyse docking scores to prioritize lead compounds, design better drug candidates, and optimize molecular structures for enhanced binding specificity. The Methyl 1,3-diphenyl-1H-naphtho[2,1-b]pyran-2-carbodithioate) is predicted to interact with metalloproteinase-13 (MMP-13) matrix, an enzyme known for its key role in degrading type II collagen, a major factor in the progression of osteoarthritis (OA)38. Its expression is detectable in healthy individuals39. Overexpression of MMP-13 in transgenic animal models leads to joint abnormalities resembling human OA. The enzymatic function of MMP-13 is implicated in conditions such as inflammatory bowel diseases, melanoma invasion, and the spread of breast cancer, highlighting its potential as a promising therapeutic target.

Table 8. Target rank of the query molecule using SwissTarget prediction

Target	Common name	Uniprot ID	ChEMBL ID	Target Class	Probability*	Known actives (3D/2D)
Matrix metalloproteinase 13	MMP13	P45452	CHEMBL280	Protease		5 / 0
Matrix metalloproteinase 8	MMP8	P22894	CHEMBL4598	Protease		3 / 0
Cannabinoid receptor 2	CNR2	P34972	CHEMBL253	Family A G protein-coupled receptor		51 / 0
11-beta-hydroxysteroid dehydrogenase 1	HSD11B1	P28845	CHEMBL4235	Enzyme		34 / 0
Adenosine A1 receptor	ADORA1	P30542	CHEMBL226	Family A G protein-coupled receptor		17 / 0
Voltage-gated potassium channel subunit Kv1.3	KCNA3	P22001	CHEMBL4633	Voltage-gated ion channel		1 / 0
Phosphodiesterase 5A	PDE5A	O76074	CHEMBL1827	Phosphodiesterase		3 / 0
Glucocorticoid receptor	NR3C1	P04150	CHEMBL2034	Nuclear receptor		45 / 0
Cannabinoid receptor 1	CNR1	P21554	CHEMBL218	Family A G protein-coupled receptor		33 / 0
Glycogen synthase kinase-3 beta	GSK3B	P49841	CHEMBL262	Kinase		4 / 0
Quinone reductase 1	NQO1	P15559	CHEMBL3623	Enzyme		2 / 0
Translocator protein *(by homology)*	TSPO	P30536	CHEMBL5742	Membrane receptor		31 / 0
15-hydroxyprostaglandin dehydrogenase [NAD+]	HPGD	P15428	CHEMBL1293255	Enzyme		7 / 0
Androgen Receptor	AR	P10275	CHEMBL1871	Nuclear receptor		7 / 0
Progesterone receptor	PGR	P06401	CHEMBL208	Nuclear receptor		28 / 0

The enzyme possesses a well-defined catalytic domain with a druggable binding site where small molecules can interact and inhibit its enzymatic function. Molecular docking is employed to discover small molecule inhibitors capable of binding to specific active sites on matrix metalloproteinase-13 (MMP-13), thereby hindering its activity. This approach is vital for the identification and optimization of candidate inhibitors with potential for clinical advancement.

The three-dimensional structure of MMP-13 is elucidated using experimental techniques like X-ray crystallography or NMR spectroscopy. This structural information informs computational docking studies, allowing predictions of how small molecules interact with MMP-13 at the atomic level. Molecular docking simulations explore the active binding conformation of MMP-18 inhibitors. Visualisation of the intermolecular interaction between the ligand (naphthopyran) and MMP-18's active sites reveals a compact complex (Figure 13). The binding scores for metalloproteinase-13 range between –4.9 and –5.9. Details of ligand–protein interactions, top-ranked compounds, and the reference drug prifinium are summarized in Table 9. The predicted binding poses of the naphthopyran derivative with metalloproteinase-13 show hydrogen bonding interactions with the amino acid residue Arg (A:109). Two distinct poses (2 and 4) exhibit bond lengths of 7.06 Å and 2.74 Å, as outlined in Table 10.

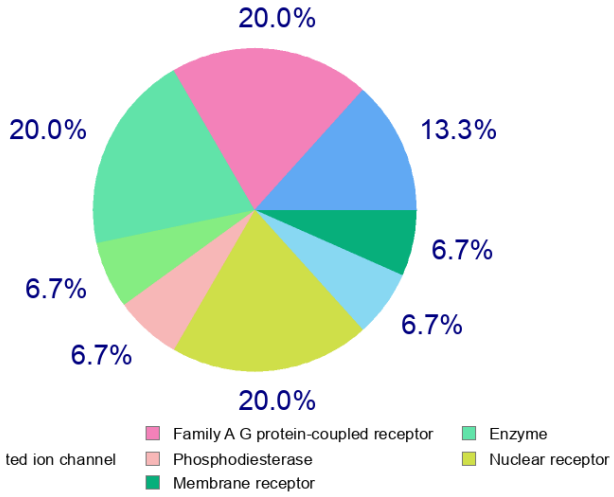

Figure 12. Pie-Chart depicting Target receptor of the Methyl 1,3-diphenyl-1H-naphtho[2,1-b]pyran-2-carbodithioate

Table 9. Target rank of the query molecule using SwissTarget prediction

Docking Pose	Docking Score	
	Naphthopyran derivative (4)	Prifinium (Standard drug)
Pose 1	-5.9	-7.0
Pose 2	-5.8	-6.2
Pose 3	-5.4	-5.7
Pose 4	-4.9	-5.3

Table 10. Type of interaction in the docking poses between query molecule and metalloproteinase-13

Pose	Type of Bond	Bond Length	Receptor Residue
POSE 1	Pi-sigma	3.78, 5.36	Arg (A:109)
	Pi-alkyl	5.16	Pro (A:108)
	Pi-cation	3.38	Arg (B:109)
	Pi-anion	4.19	Asp (B:231)

	Van der waals		Phe (B:107), His(A:232), Asp(A:231), Pro (B:190), Phe(A:107), Lys(A:284), His (B:232)
POSE 2	Pi-alkyl Hydrogen-bond Van der waals	6.08 {5.87 6.35} 7.06	Pro (A:242) {Lys (A:234) Arg (A:109)} Arg (B:109) {His(A:232), His(A:226), Asp(A:231), Phe (B:107), Pro(B:190), Pro(A:108), Phe(A:107), Asp(B:231), Ser (A:233)}
POSE 3	Pi-alkyl Pi-cation Pi-anion Van der waals	5.84 {5.41 7.12 6.52} 7.01	Arg (A:109), {Asp (A:231) Arg (B:109) Arg (B:109)} Phe (A:107) {Pro(A:108), Phe(B:107), His(A:226), His(A:232), Lys(A:234)}
POSE 4	Pi-alkyl Pi-cation Pi-anion Hydrogen Bond Vander waals	Not observed {3.59 3.30 4.87} 4.09 2.74	 {Lys (A:234) Lys (A:234) Asp (A:231)} Arg (B:109) Arg (B:109) {Phe (A:107), Ser(A:233), Pro (A:242), His(A:232), Phe (B:107), Asp(B:231), Arg (A:109)}

Figure 13. Different poses of docking of the query molecule within MMP-13

Conclusion

The study on Methyl 1,3-diphenyl-1H-naphtho[2,1-b]pyran-2-carbodithioate exhibits high chemical stability and low reactivity, indicated by its high HOMO-LUMO gap and moderate dipole moment of the compound. Despite its overall stability, certain regions identified by the Fukui function and MEP analysis may still be reactive under specific conditions. The ADME analysis reveals challenges for pharmaceutical applications due to low oral bioavailability, poor solubility, and lack of blood-brain barrier permeability. Molecular docking studies suggest potential interaction with MMP-13, a target involved in osteoarthritis and other diseases. However, the compound's development as a therapeutic agent is hindered by its

Figure 13: Different poses of docking of the query molecule within MMP-13

pharmacokinetic issues. Future research should focus on modifying the molecule to enhance its drug-like properties while retaining its ability to interact with MMP-13 or similar targets.

These computational and spectroscopic findings establish methyl 1,3-diphenyl-1H-naphtho[2,1-b]pyran-2-carbodithioate as a stable, pharmacologically relevant scaffold, providing a basis for further lead optimization.

Acknowledgement: The authors gratefully acknowledge the Head of the Chemistry Department, D.M. College of Science, Dhanamanjuri University, Manipur, India, for kindly providing access to the laboratory facilities, which were vital to the completion of this study.

Conflict of Interest: The authors declare that there are no conflicts of interest.

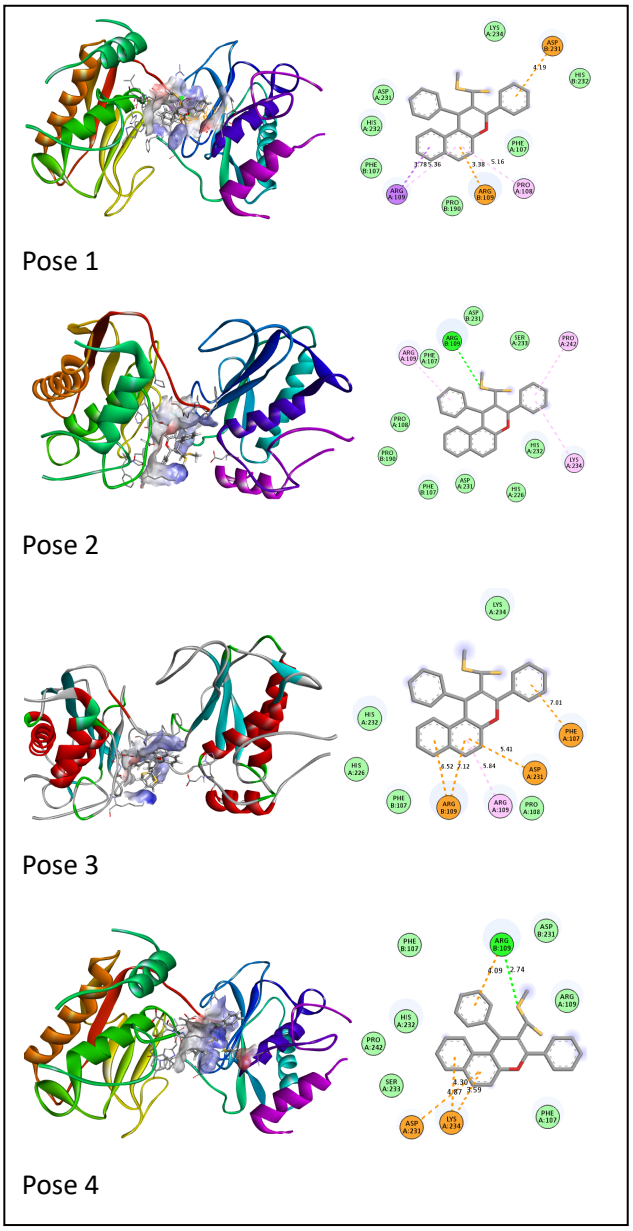

Compliance with Ethical Standards: This article does not contain any studies involving human or animal subjects.

REFERENCE

[1] Devi AK, Chanu LG, Chanu IH, Singh OM. ChemInform Abstract: One-Pot Synthesis of 1H-Naphtho[2,1-b]pyran Derivatives under Solvent-Free Conditions. ChemInform. 015;46(20):chin.201520165.doi:10.1002/chin.201520165

[2] Kuroiwa H, Inagaki Y, Mutoh K, Abe J. On-Demand Control of the Photochromic Properties of Naphthopyrans. Advanced Materials. 2019;31(2):1805661. doi:10.1002/adma.201805661

[3] Brazevic S, Sliwa M, Kobayashi Y, Abe J, Burdzinski G. Disclosing Whole Reaction Pathways of Photochromic 3 H -Naphthopyrans with Fast Color Fading. J Phys Chem Lett. 2017;8(5):909-914. doi:10.1021/acs.jpclett.6b03068

[4] Schmitt F, Gold M, Rothemund M, Andronache I, Biersack B, Schobert R, et al. New naphthopyran analogues of LY290181 as potential tumor vascular-disrupting agents. European Journal of Medicinal Chemistry. 2019;163:160-168. doi:10.1016/j.ejmech.2018.11.055

[5] El-Mawgoud HKA, Radwan HAM, Fouda AM, El-Mariah F, Elhenawy AA, Amr AE, et al. Synthesis, cytotoxic activity, crystal structure, DFT, molecular docking study of some heterocyclic compounds incorporating benzo[f]chromene moieties. Journal of Molecular Structure. 2022;1260:132829. doi:10.1016/j.molstruc.2022.132829

[6] Ojha M, Kumar A, Prasun C, Nair MS, Chaturvedi S, Paliwal SK, et al. Synthesis, characterization, and in silico studies of 1,8-naphthyridine derivatives as potential anti-Parkinson's agents. Journal of Biomolecular Structure and Dynamics. 2023;41(3):805-820. doi:10.1080/07391102.2021.2013320

[7] Kurbanova MM, Maharramov AM, Sadigova AZ, Gurbanova FZ, Mali SN, Al-Salahi R, et al. Synthesis, Characterization, DFT, and In Silico Investigation of Two Newly Synthesized β-Diketone Derivatives as Potent COX-2 Inhibitors. Bioengineering. 2023;10(12):1361. doi:10.3390/bioengineering10121361

[8] Neese F, Wennmohs F, Becker U, Riplinger C. The ORCA quantum chemistry program package. The Journal of Chemical Physics. 2020;152(22):224108. doi:10.1063/5.0004608

[9] Sarotti AM, Pellegrinet SC. Application of the Multi-standard Methodology for Calculating 1 H NMR Chemical Shifts. J Org Chem. 2012;77(14):6059-6065. doi:10.1021/jo3008447

[10] Defant A, Mancini I. A Comprehensive Computational NMR Analysis of Organic Polyarsenicals including the Marine Sponge-Derived Arsenicins A–D and Their Synthetic Analogs. Marine Drugs. 2023;21(10):511. doi:10.3390/md21100511

[11] Isravel AD, Jeyaraj JK, Thangasamy S, John WJ. DFT, NBO, HOMO-LUMO, NCI, stability, Fukui function and hole – Electron analyses of tolcapone. Computational and Theoretical Chemistry. 2021;1202:113296. doi:10.1016/j.comptc.2021.113296

[12] Jamróz MH. Vibrational Energy Distribution Analysis (VEDA): Scopes and limitations. Spectrochimica Acta Part A: Molecular and Biomolecular Spectroscopy. 2013;114:220-230. doi:10.1016/j.saa.2013.05.096

[13] Darugar V, Vakili M, Tayyari SF, Kamounah FS. Validation of potential energy distribution by VEDA in vibrational assignment some of β-diketones; comparison of theoretical predictions and experimental vibration shifts upon deutration. Journal of Molecular Graphics and

Modelling. 2021;107:107976. doi:10.1016/j.jmgm.2021.107976

[14] Lu T, Chen F. Multiwfn: A multifunctional wavefunction analyzer. J Comput Chem. 2012;33(5):580-592. doi:10.1002/jcc.22885

[15] Gfeller D, Grosdidier A, Wirth M, Daina A, Michielin O, Zoete V. SwissTargetPrediction: a web server for target prediction of bioactive small molecules. Nucleic Acids Research. 2014;42(W1):W32-W38. doi:10.1093/nar/gku293

[16] Daina A, Michielin O, Zoete V. SwissADME: a free web tool to evaluate pharmacokinetics, drug-likeness and medicinal chemistry friendliness of small molecules. Sci Rep. 2017;7(1):42717. doi:10.1038/srep42717

[17] Lipinski CA, Lombardo F, Dominy BW, Feeney PJ. Experimental and computational approaches to estimate solubility and permeability in drug discovery and development settingsq. Advanced Drug Delivery Reviews. Published online 2001.

[18] Ghose AK, Viswanadhan VN, Wendoloski JJ. A Knowledge-Based Approach in Designing Combinatorial or Medicinal Chemistry Libraries for Drug Discovery. 1. A Qualitative and Quantitative Characterization of Known Drug Databases. J Comb Chem. 1999;1(1):55-68. doi:10.1021/cc9800071

[19] Veber DF, Johnson SR, Cheng HY, Smith BR, Ward KW, Kopple KD. Molecular Properties That Influence the Oral Bioavailability of Drug Candidates. J Med Chem. 2002;45(12):2615-2623. doi:10.1021/jm020017n

[20] Egan WJ, Merz, KM, Baldwin JJ. Prediction of Drug Absorption Using Multivariate Statistics. J Med Chem. 2000;43(21):3867-3877. doi:10.1021/jm000292e

[21] Muegge I, Heald SL, Brittelli D. Simple Selection Criteria for Drug-like Chemical Matter. J Med Chem. 2001;44(12):1841-1846. doi:10.1021/jm015507e

[22] Delaney JS. ESOL: Estimating Aqueous Solubility Directly from Molecular Structure. J Chem Inf Comput Sci. 2004;44(3):1000-1005. doi:10.1021/ci034243x

[23] Ali J, Camilleri P, Brown MB, Hutt AJ, Kirton SB. In Silico Prediction of Aqueous Solubility Using Simple QSPR Models: The Importance of Phenol and Phenol-like Moieties. J Chem Inf Model. 2012;52(11):2950-2957. doi:10.1021/ci300447c

[24] Shankar R, Senthilkumar K, Kolandaivel P. Calculation of ionization potential and chemical hardness: A comparative study of different methods. Int J of Quantum Chemistry. 2009;109(4):764-771. doi:10.1002/qua.21883

[25] Mumit MA, Pal TK, Alam MA, Islam MAAAA, Paul S, Sheikh MC. DFT studies on vibrational and electronic spectra, HOMO–LUMO, MEP, HOMA, NBO and molecular docking analysis of benzyl-3-N-(2,4,5-trimethoxyphenylmethylene)hydrazinecarbodithioate. Journal of Molecular Structure. 2020;1220:128715. doi:10.1016/j.molstruc.2020.128715

[26] Rijal R, Lamichhane HP, Pudasainee K. Molecular structure, homo-lumo analysis and vibrational spectroscopy of the cancer healing pro-drug temozolomide based on dft calculations. AIMSBPOA. 2022;9(3):208-220. doi:10.3934/biophy.2022018

[27] Hait D, Head-Gordon M. How Accurate Is Density Functional Theory at Predicting Dipole Moments? An Assessment Using a New Database of 200 Benchmark Values. J Chem Theory Comput. 2018;14(4):1969-1981. doi:10.1021/acs.jctc.7b01252

[28] Politzer P, Murray JS. Molecular Electrostatic Potentials: Significance and Applications. In: Chattaraj PK, Chakraborty D, eds. Chemical Reactivity in Confined Systems. 1st ed. Wiley; 2021:113-134. doi:10.1002/9781119683353.ch7

[29] Singh NS, Devi SM. Computational Exploration of 1-Amidino-O-(n-butyl) Urea (ABnUH) with Natural AtomicOrbitals, Natural Bond Orbital, Vibrational Analysis and Simulated UV-Visible Spectra. Asian J Chem. 2021;33(12):3089-3098. doi:10.14233/ajchem.2021.23438

[30] Palafox MA. DFT computations on vibrational spectra: Scaling procedures to improve the wavenumbers. Physical Sciences Reviews. 2018;3(6). doi:10.1515/psr-2017-0184

[31] Allison TC, Tong YJ. Application of the condensed Fukui function to predict reactivity in core–shell transition metal nanoparticles. Electrochimica Acta. 2013;101:334-340. doi:10.1016/j.electacta.2012.12.072

[32] Zamora PP, Bieger K, Cuchillo A, Tello A, Muena JP. Theoretical determination of a reaction intermediate: Fukui function analysis, dual reactivity descriptor and activation energy. Journal of Molecular Structure. 2021;1227:129369. doi:10.1016/j.molstruc.2020.129369

[33] Choudhary K, Garrity KF, Camp C, Kalinin SV, Vasudevan R, Ziatdinov M, et al. Computational scanning tunneling microscope image database. Sci Data. 2021;8(1):57. doi:10.1038/s41597-021-00824-y

[34] Cheeseman JR, Trucks GW, Keith TA, Frisch MJ. A comparison of models for calculating nuclear magnetic resonance shielding tensors. The Journal of Chemical Physics. 1996;104(14):5497-5509. doi:10.1063/1.471789

[35] Szczepanik D, Mrozek J. On several alternatives for Löwdin orthogonalization. Computational and Theoretical Chemistry. 2013;1008:15-19. doi:10.1016/j.comptc.2012.12.013

[36] Sarkar D, Maiti AK, Alenazy R, Joseph B. In silico Approach to Identify Potent Bioactive Compounds as Inhibitors against the Enoyl-acyl Carrier Protein (acp) Reductase Enzyme of Mycobacterium tuberculosis.

Biointerface Res Appl Chem. 2021;12(5):7023-7039. doi:10.33263/BRIAC125.70237039

[37] Mateev E, Kondeva-Burdina M, Georgieva M, Mateeva A, Valkova I, Tzankova V, et al. Synthesis, Biological Evaluation, Molecular Docking and ADME Studies of Novel Pyrrole-Based Schiff Bases as Dual Acting MAO/AChE Inhibitors. Sci Pharm. 2024;92(2):18. doi:10.3390/scipharm92020018

[38] Choi JY, Fuerst R, Knapinska AM, Taylor AB, Smith L, Cao X, et al. Structure-Based Design and Synthesis of Potent and Selective Matrix Metalloproteinase 13 Inhibitors. J Med Chem. 2017;60(13):5816-5825. doi:10.1021/acs.jmedchem.7b00514

[39] Bau B, Gebhard PM, Haag J, Knorr T, Bartnik E, Aigner T. Relative messenger RNA expression profiling of collagenases and aggrecanases in human articular chondrocytes in vivo and in vitro. Arthritis & Rheumatism. 2002;46(10):2648-2657. doi:10.1002/art.10531